J Mater Sci (2012) 47:234–240
DOI 10.1007/s10853-011-5790-3

An investigation into the capability of unconventional amount of aluminum and nano-alumina to alter the mechanical response of magnesium

Q. B. Nguyen · Yi Fan · K. S. Tun · J. Chan · R. Kwok · J. V. M. Kuma · M. Gupta

Received: 8 June 2011 / Accepted: 12 July 2011 / Published online: 23 July 2011

Abstract In the present study, magnesium aluminum alloys with aluminum content exceeding conventional alloying limit (Mg–10Al, Mg–15Al, and Mg–20Al) and the composite of Mg–10Al alloy with 1.5 volume percentage of nano-alumina particulates are created using the technique of disintegrated melt deposition. Significant improvements in microstructure and mechanical properties compared with pure magnesium are obtained. Intermetallic phase $Mg_{17}Al_{12}$ was detected in all the materials. The increase in amount of aluminum in magnesium led to a reduction in coefficient of thermal expansion and a marginal increase in porosity. Yield strength, ultimate tensile strength, and hardness increased significantly with an increasing amount of aluminum. The 0.2% yield strength increased from 140 to 394 MPa (181%) in the case of Mg–20Al. Ductility reduced with progressive addition of aluminum. However, the addition of both Al and nano-alumina particulates significantly increased not only strengths, but also ductility of pure Mg. The overall tensile properties assessed in terms of work of fracture increased by almost 143% in the case of composite sample. An attempt is made in this study to correlate the tensile response of alloys and composite with their microstructural characteristics.

Q. B. Nguyen · Y. Fan · K. S. Tun · M. Gupta (✉)
Department of Mechanical Engineering, National University of Singapore, 9 Engineering Drive 1, Singapore 117576, Singapore
e-mail: mpegm@nus.edu.sg

J. Chan · R. Kwok
Singapore Technologies Kinetics Ltd (ST Kinetics), 249 Jalan Boon Lay, Singapore 619523, Singapore

J. V. M. Kuma
Minerals, Metals & Materials Technology Centre, National University of Singapore, 9 Engineering Drive 1, Singapore 117576, Singapore

Introduction

Magnesium alloys and its composites have been intensively developed during the last two decades for weight critical applications, such as in automotive, aerospace, electronics, defense, and sports industries. Magnesium-based materials are targeted as they are approximately 35% lighter than aluminum, 61% lighter than titanium, and 78% lighter than iron [1–3]. In addition, magnesium-based materials exhibit some advantages, such as the highest strength to weight ratio of any of the commonly used structural materials, good castability, and machinability [4, 5]. Further, they have good dimensional stability and electromagnetic shielding capability [6, 7]. However, their main disadvantages include low stiffness, limited ductility, and poor corrosion resistance [4–8].

The literature search shows that there are several systems of magnesium alloys: magnesium–aluminum–manganese with and without zinc (AM and AZ), magnesium–zirconium (K), magnesium–zinc–zirconium with and without rare earths (ZK, ZE and EZ), magnesium–thorium–zirconium with and without zinc (HK, HZ, and ZH), magnesium–silver–zirconium with rare earths or thorium (QE and QH), magnesium–yttrium–rare earth–zirconium (WE), and magnesium–zinc–copper–manganese (ZC) [9]. Amongst these systems, AZ (magnesium–aluminum) system has more advantages including casting ability, high mechanical properties, and cost savings [9–11]. It is well known that Al has good metallurgical compatibility with Mg [1, 9]. Effect of aluminum element on mechanical properties of magnesium has been thoroughly investigated for the amounts of aluminum ranging from 0 to 9 wt% and accordingly commercially available AZ alloys are designated as AZ31, AZ60, AZ61, AZ80, and AZ91 [9]. There has been limited research on the

effect of the amount of aluminum on the properties of magnesium beyond 9 wt% [3]. The literature search in recent years also reveals that many attempts have been made to further enhance the properties of AZ alloys by adding alloying elements, such as Ti, Y, Ca, Gd, Si, and Zr [6–8, 10–14] or reinforcing with ceramic particulates such as micro-SiC particulates, nano-Y_2O_3, nano-Al_2O_3, etc. [15–18]. Among these ceramic particulate reinforcements, addition of nano-Al_2O_3 improves the failure strain of AZ31 magnesium alloys remarkably. However, no attempt is made so far to improve the overall mechanical properties of pure Mg by the addition of high amount of aluminum and reinforcing it with nano-Al_2O_3 ceramic particulates using the industrially viable solidification method.

Accordingly, in the present study an attempt is made to add aluminum beyond conventionally alloying limit to improve microstructural characteristics, hardness and strength of magnesium, and nano-alumina particulates to improve failure strain of the selected magnesium–aluminum system. Disintegrated melt deposition technique (DMD) is used in the present study to synthesize these materials, and all the characterization studies were performed on the extruded specimens.

Materials preparation and experimental procedures

In the present study, pure magnesium billet with purity of 99.9% was used as matrix material. Aluminum powder (supplied by Alfa Aesar's company with purity of 99.9%) was used for alloying purpose, while 50 nm-alumina particulates (supplied by Baikowski (Japan) with purity of 99.9%) were used as reinforcement phase. Arrays of holes with 10-mm diameter and 50-mm depth were CNC machined in the pure magnesium blocks to contain Al and nano-Al_2O_3 powders. Three different weight percentages of Al (10, 15, and 20 wt%) were selected for alloying with pure magnesium. 1.5 vol% of 50 nm Al_2O_3 particulates was added in Mg–10Al as this alloy exhibited the best combination of strength and failure strain amongst the above three alloys.

The 40-mm-diameter ingots of pure Mg, Mg–10Al, Mg–15Al, Mg–20Al, and Mg–10Al–1.5Al_2O_3 were produced using the DMD technique which is fully described elsewhere [5]. Ingots were subsequently machined to 36-mm diameter and hot extruded at 350 °C to 8-mm-diameter rods. All the characterization studies including density measurement, X-ray, microstructure, coefficient of thermal expansion, microhardness, tensile testing, and fracture analysis were carried out on the extruded samples.

Results and discussion

Macrostructural observation

Pure Mg, Mg–10Al, Mg–15Al, Mg–20Al, and Mg–10Al–1.5Al_2O_3 samples were successfully synthesized using DMD technique followed by hot extrusion. Macrostructural characterization studies conducted on these samples did not reveal any presence of macrodefects. Solidification shrinkage cavities were absent in the preforms. Following extrusion, there was also no evidence of any macrostructural defects. These results are consistent with the previous findings made on magnesium-based materials processed using DMD technique [3, 15, 18, 19].

Microstructural characterization

Figure 1 shows the X-ray diffractograms of Mg, Mg–10Al, Mg–15Al, Mg–20Al, and Mg–10Al–1.5Al_2O_3 samples. The secondary phase $Mg_{17}Al_{12}$ was formed in all the alloys and composite samples. However, none of the nano-alumina peaks was detectable due to its limited volume fraction and nano-length scale [19]. The morphology of secondary phase $Mg_{17}Al_{12}$ can be clearly assessed from Fig. 2. This secondary phase is predominantly located at the grain boundaries (Figs. 2, 3). Scion Image Analysis Software was employed to quantify the amount of secondary phase, and the results are shown in Table 1. It indicates that the amount of secondary phase $Mg_{17}Al_{12}$ increases with an increase in the amount of Al. This finding is consistent with the previous observation made by El-Amoush [10]. The presence of nano-alumina assisted in breaking the network of secondary phase and dispersing it in magnesium matrix (Fig. 2d). Microstructural studies conducted on the extruded samples revealed reasonably uniform distribution of the secondary phase $Mg_{17}Al_{12}$ in the case of Mg–10Al and Mg–10Al–1.5Al_2O_3 samples. However, the secondary phase tends to increasingly form clusters with the increasing presence of Al (Fig. 2b, c). This observation is clearly seen in the case of Mg–20Al (Fig. 2c).

The results of microstructural characterization revealed presence of nearly equiaxed grains (Fig. 3) in all the samples. Scion image processing software was employed to analyze grain size and aspect ratio. The results are presented in Table 1. The grain size is roughly 18 μm in the case of pure Mg and it is much smaller (5–7 μm) when Al and nano-alumina is added. The presence of Al led to a significant decrease in grain size suggesting the capability of $Mg_{17}Al_{12}$ to serve as either nucleation sites or obstacles to grain growth during solid state cooling [5]. Further, but marginal reduction in average grain size was obtained when both Al and nano-alumina was added in pure Mg.

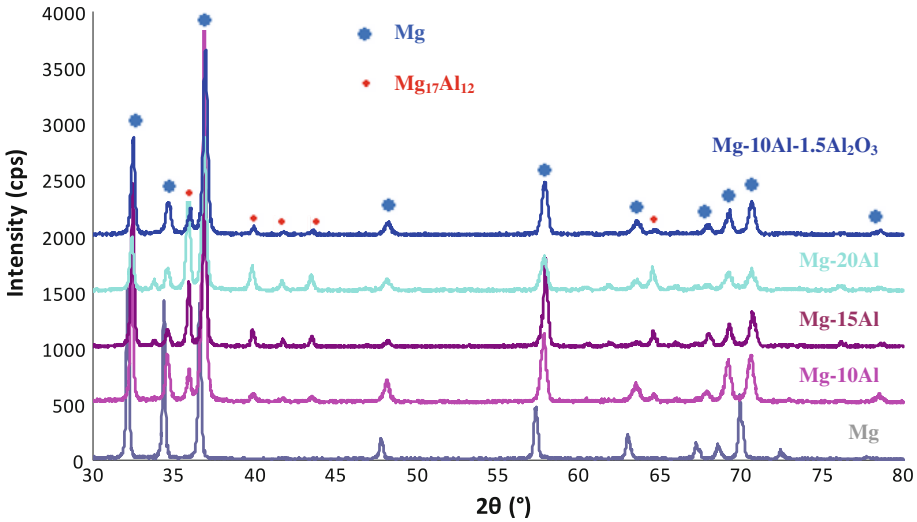

Fig. 1 X-ray diffractograms of Mg, Mg–10Al, Mg–15Al, Mg–20Al, and Mg–10Al–$1.5Al_2O_3$ samples

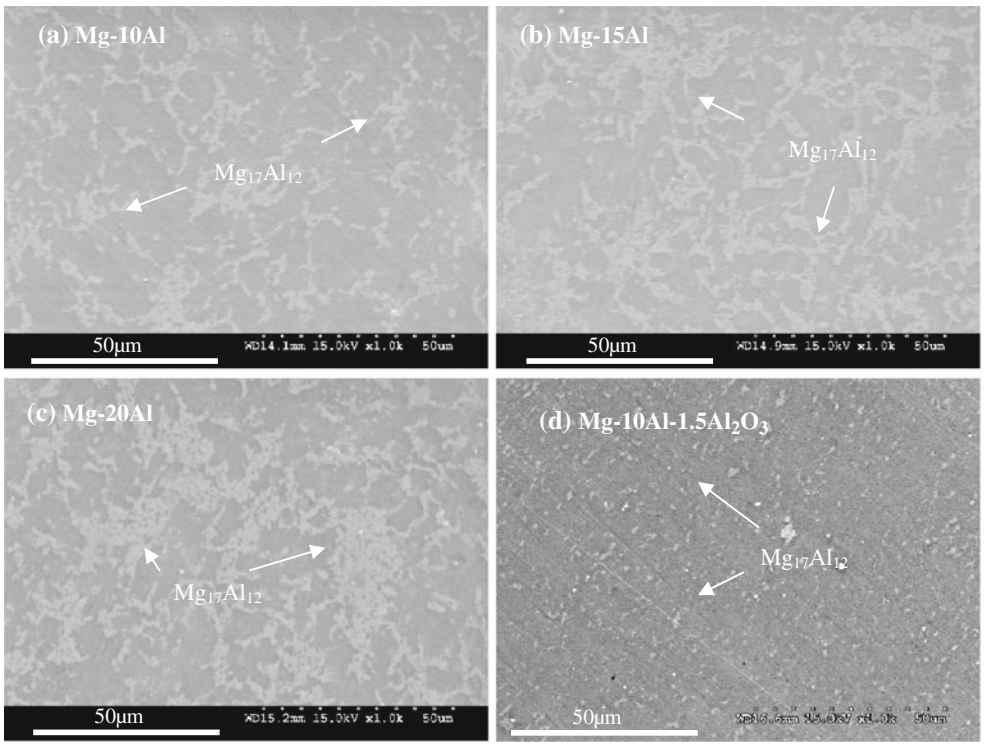

Fig. 2 Representative FESEM micrographs showing the distribution characteristics of secondary phase

Table 1 Experimental results of density and porosity measurements

Material	Vol. of intermetallic (%)	Grain size (μm)	Aspect ratio	Density (g/cm^3)		Porosity (%)
				Theo.	Experimental	
Mg	0	17.71 ± 6.59	1.38	1.740	1.739 ± 0.004	0.06
Mg–10Al	8.42 ± 1.05	6.59 ± 1.72	1.38	1.804	1.793 ± 0.004	0.10
Mg–15Al	11.68 ± 1.24	5.82 ± 1.60	1.52	1.838	1.836 ± 0.003	0.12
Mg–20Al	14.85 ± 0.79	5.65 ± 1.40	1.39	1.873	1.866 ± 0.001	0.17
Mg–10Al–$1.5Al_2O_3$	8.64 ± 1.36	5.34 ± 1.06	1.45	1.839	1.833 ± 0.003	0.08

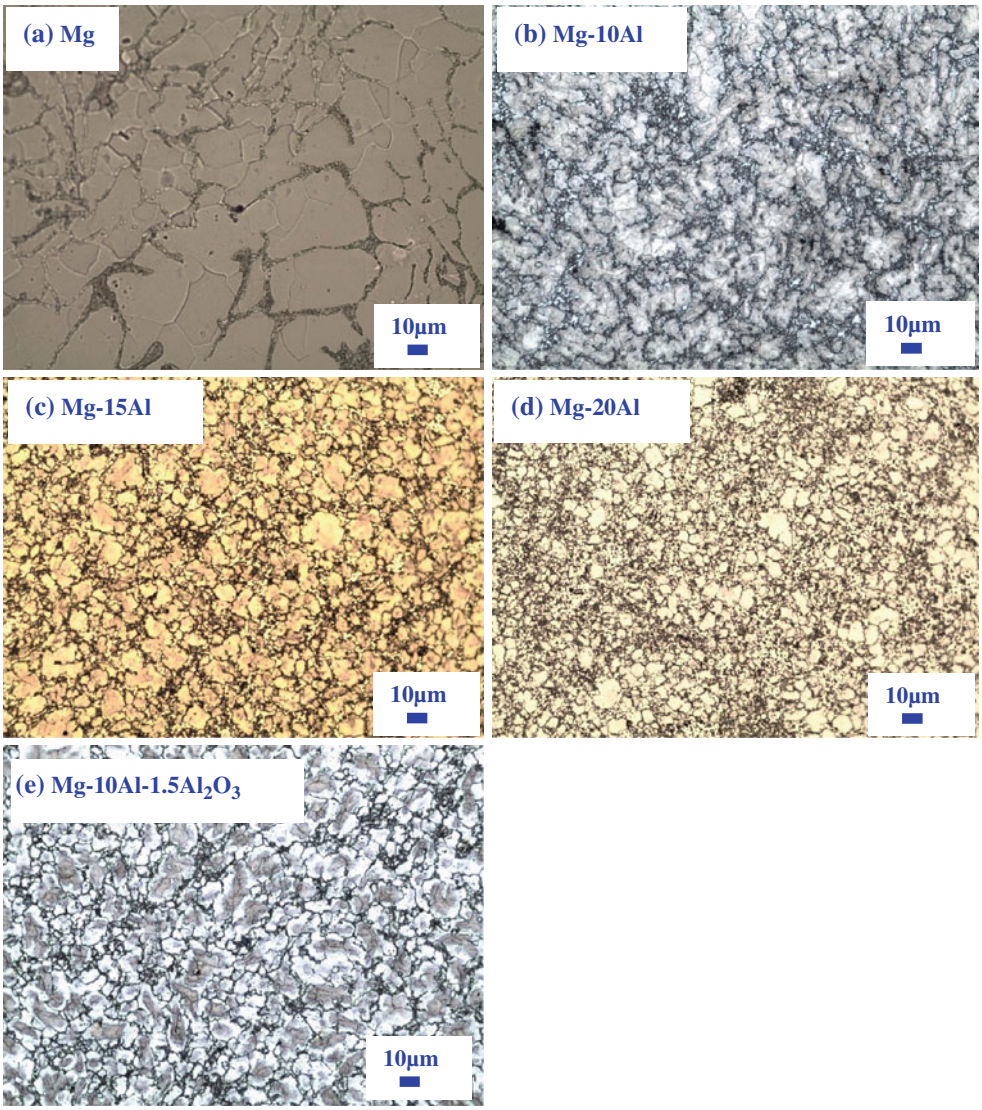

Fig. 3 Grain morphology of **a** Mg, **b** Mg–10Al, **c** Mg–15Al, **d** Mg–20Al, and **e** Mg–10Al–1.5Al_2O_3 samples

The microstructural characterization reveals the presence of minimal porosity in all the samples (see Figs. 2, 3). This is also supported by the porosity results obtained using density measurement (Table 1). The porosity increased marginally with an increase in the amount of Al but remained quite low. Presence of minimal porosity can be attributed to (i) good compatibility between Mg matrix and intermetallic/reinforcement, leading to the absence of voids and debonded regions usually associated with them [16], and (ii) judicious selection of experimental parameters during primary and secondary processing [3]. These results suggest homogeneous microstructure in terms of distribution of porosity, intermetallic phase and where applicable the Al_2O_3 particulates.

Microstructural characterization of alloys and composite samples also indicated a near defect-free interface formed between secondary phases and the matrix (see Fig. 2). The interfacial integrity was assessed in terms of interfacial debonding and the presence of microvoids at the interface. It is established that Mg has good metallurgical compatibility with Al [1, 9]. Further, previous finding showed good wettability of nano-Al_2O_3 particulates by the magnesium-based matrices [3, 13, 16].

Coefficient of thermal expansion

Figure 4 shows the results of the coefficient of thermal expansion measurements obtained from pure Mg and its alloys and composite samples using the TMA PT 1000 model. The results exhibited a significant reduction in CTE of pure Mg with an increase in the amount of Al and due to presence of nano-Al_2O_3 particulates. The CTE values obtained in the present study are lower compared with AZ31, AZ61, AZ80, and AZ91 [9]. The progressive

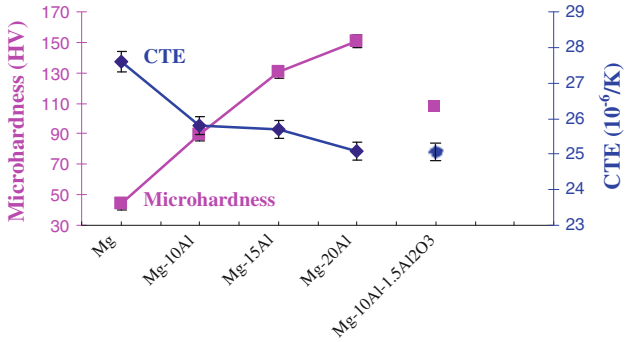

Fig. 4 Results of microhardness and CTE measurement of samples

reduction in CTE of Mg with an increase in the amount of Al may be attributed to the increasing presence of secondary phase $Mg_{17}Al_{12}$ [5]. The reduction in CTE in the case of composite sample can be attributed to much lower CTE value of alumina when compared with pure Mg (28.9×10^{-6} and 7.4×10^{-6} K^{-1} for pure Mg and Al_2O_3, respectively) and the ability of the reinforcement particulates to effectively constrain the expansion of the matrix [9, 19]. The results of this study suggest that both Al and Al_2O_3 enhance the dimensional stability of pure Mg.

Hardness

The results of microhardness measurements using Shimadzu-HMV automatic digital microhardness tester revealed a significant increase in average microhardness with an increase in the amount of Al and nano-alumina particulates (see Fig. 4). The increase in hardness of samples with increasing amount of Al and nano-alumina can be attributed primarily to (i) an increase in the presence of harder intermetallic phases $Mg_{17}Al_{12}$ with an increase in amount of Al, (ii) greater constraint on localized matrix deformation during indentation due to the presence of reinforcement phase in the case of composite sample (see Fig. 2) [19], and (iii) progressive reduction in grain size with an increase in amount of Al and reduction in grain size due to the presence of nano-Al_2O_3. The results are consistent with the earlier observations made elsewhere [5, 19].

Tensile characteristics

MTS 810 tensile testing machine attached with an extensometer was employed to assess tensile response of samples. The results are shown in Table 2 and Fig. 5. The addition of Al led to remarkable improvement in yield strength and ultimate strength of pure Mg. The yield strength increased from 140 to 389 MPa (178% increment), the ultimate strength increased from 193 to 402 MPa (108% increment) in the case of Mg–20Al. In contrast, failure strain was significantly compromised with

Table 2 Results of tensile properties of samples at room temperature

Material	0.2YS (MPa)	UTS (MPa)	FS (%)	WoF (MJ/m^3)
Mg	140 ± 5	193 ± 2	7.7 ± 0.1	14.5 ± 0.5
Mg–10Al	228 ± 7	329 ± 9	6.6 ± 1.4	22.0 ± 4.8
Mg–15Al	305 ± 6	344 ± 2	2.2 ± 1.0	8.5 ± 3.4
Mg–20Al	389 ± 9	402 ± 14	0.3 ± 0.0	3.5 ± 0.3
Mg–10Al–$1.5Al_2O_3$	241 ± 11	352 ± 10	9.2 ± 1.2	35.2 ± 3.3
AZ31B [5]	201 ± 7	270 ± 6	5.6 ± 1.4	–
AZ91 [19]	272 ± 3	353 ± 0	3.7 ± 0.5	–
Mg–$1.1Al_2O_3$ [20]	194 ± 5	250 ± 3	6.9 ± 1.0	–

an increase in amount of Al. However, improvement in strengths and ductility were both achieved with the simultaneous addition of Al and nano-alumina in the case of Mg–10Al–$1.5Al_2O_3$ sample. The yield strength, ultimate strength, and failure strain improved from 140 to 241 MPa, 193 to 352 MPa, and 7.7 to 9.2%, respectively. The net outcome was an enhanced work of fracture of Mg–10Al–$1.5Al_2O_3$ from 14.5 to 35.2 MJ/m^3 (143% increment), when compared with pure Mg (see Table 2; Fig. 5). The results indicated much improvement in mechanical properties compared with the similar study reported elsewhere [5, 10].

The significant increase in 0.2% yield strength and ultimate tensile strength of pure Mg due to the addition of Al and nano-alumina particulates can be primarily attributed to (i) grain refinement (see Table 1) [10], (ii) the increasing presence of reasonably distributed harder secondary phase/particulates [15], (iii) the effective load transfer between matrix and secondary phases [18], and (iv) the formation of internal stresses due to different thermal expansion behavior between $Mg_{17}Al_{12}$/particulates and the Mg matrix [19].

A reduction in failure strain was observed with an increase in the amount of Al (see Table 2; Fig. 5). This can primarily be attributed to (i) increasing amount of secondary

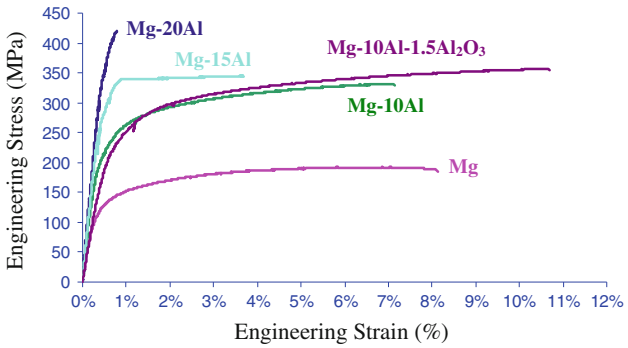

Fig. 5 Tensile stress–strain curves of samples

phase $Mg_{17}Al_{12}$ in the Mg matrix which leads to plastic incompatibility and serves as potential crack initiation sites [15], (ii) progressive increase in agglomeration tendency of secondary phase $Mg_{17}Al_{12}$ (see Fig. 2), and (iii) an increase in porosity level with an increase in amount of Al [1].

Table 2 also shows the increase in failure strain of pure Mg when Al and nano-alumina particulates were simultaneously added. An increment of 19.5% in failure strain was recorded in the case of Mg–10Al–1.5Al_2O_3 when compared with pure Mg sample. The increase in failure strain can primarily be attributed to (a) grain refinement (see Table 1) [21], and (b) presence and reasonably good distribution of secondary phase/particulates [5]. Previous findings showed that grain refinement particularly benefits hexagonal metals in ductility increment [19]. The increase in ductility of brittle materials such as magnesium can also be attributed to the presence of nano-size particulates such as Al_2O_3 and Y_2O_3 [5, 17, 19]. It has also been established before that breakdown of the secondary phase located at grain boundaries and the change in their distribution from a predominantly aggregated type to dispersed type assists in improving ductility (see Fig. 3b) [5].

A significant increment in work of fracture was observed in the case of Mg–10Al and Mg–10Al–1.5Al_2O_3 samples when compared with pure Mg sample. Work of fracture increased from 14.5 to 22 MJ/m^3 and 35.2 MJ/m^3 in the case of Mg–10Al and Mg–10Al–1.5Al_2O_3 samples, respectively. This is equivalent to an increment of up to 143%. The increase in work of fracture can mainly be attributed to the improved strengths (0.2%YS and UTS) of Mg–10Al with a marginal compromise in failure strain and to the significant improvement in both strengths and failure strain of Mg–10Al–1.5Al_2O_3 samples. Work of fracture expresses the ability of material to absorb energy up to

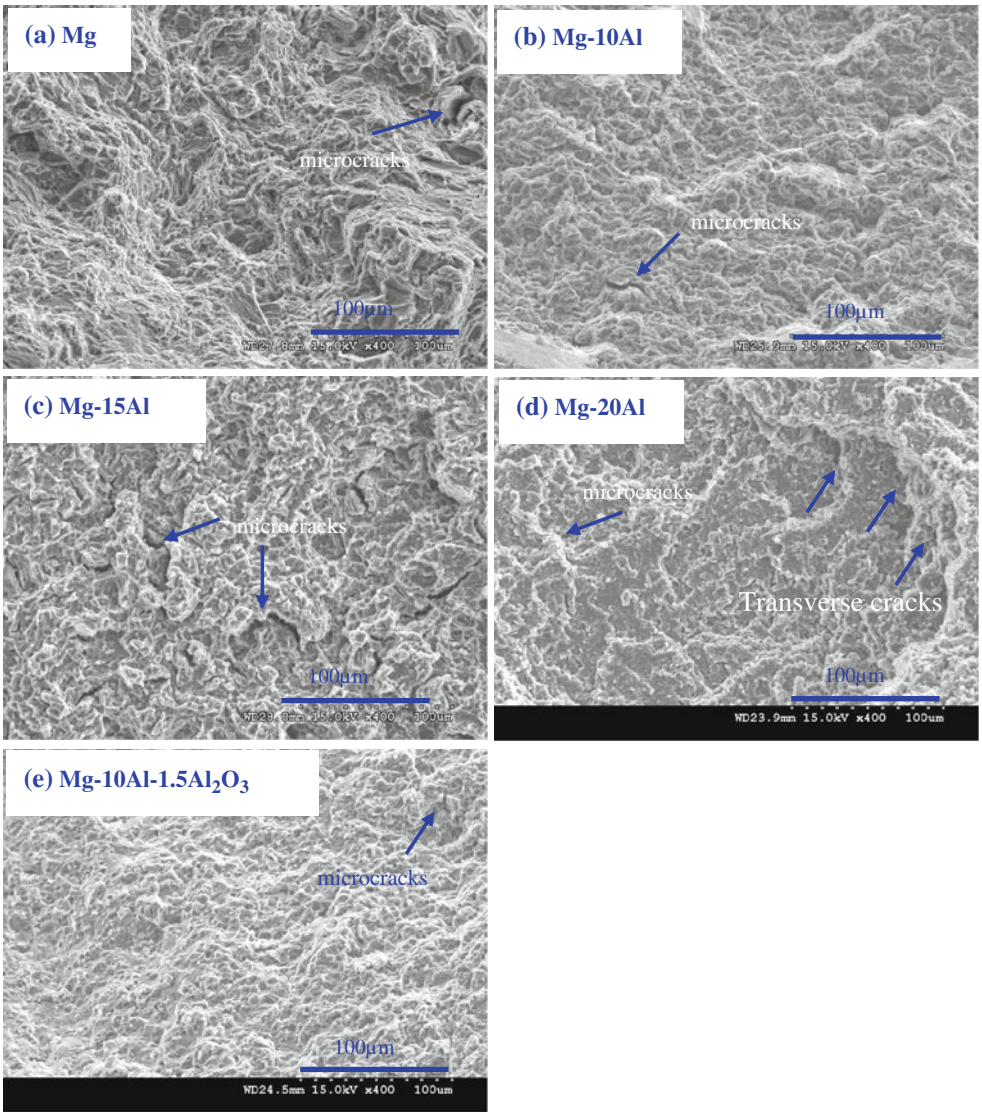

Fig. 6 Fractographs showing fracture characteristics of samples

fracture under tensile load and corresponds to the area under engineering stress–strain curve [18]. The results, thus, clearly reveal the enhanced damage tolerant capability of Mg–10Al and Mg–10Al–1.5Al_2O_3 formulations.

Comparison of the tensile properties with that of Mg–Al system (AZ series) reveals that the monolithic materials developed in this study (10Al to 20Al) exhibit superior strength but limited ductility. In the case of Mg–10Al–1.5Al_2O_3 composite, significantly higher strength and ductility were achieved compared with that of Mg/Al_2O_3 composite (Table 2).

Fracture behavior

The tensile fracture surface morphology of pure Mg, its alloys, and composite material is shown in Fig. 6. The study of uniaxially deformed fracture surfaces indicated the microstructural effects on fracture characteristics of samples. Pure Mg, Mg–10Al, and Mg–10Al–1.5Al_2O_3 samples showed mixed-mode fracture, presence of microcracks, and evidence of plastic deformation [21, 22]. Limited number of microcracks was observed in the case of Mg, Mg–10Al samples while comparatively shorter and finer microcracks were observed in the case of Mg–10Al–1.5Al_2O_3 sample. This also explains the question of why higher failure strain was obtained in the case of Mg–10Al–1.5Al_2O_3 sample. However, the fracture mode was found to be much different in the case of Mg–15Al and Mg–20Al samples. In the case of Mg–15Al sample, bigger microcracks were observed with very rough fracture surface. Microcracks and transverse microcracks were observed in the case of Mg–20Al samples. In addition, flat fracture surface was observed in the case of Mg–20Al samples [21]. These explain the reason of low failure strain or ductility in the case of Mg–15Al and Mg–20Al samples.

Conclusions

The main conclusions that may be derived from this study are as follows:

1. The disintegrated melt deposition technique coupled with hot extrusion can be employed to synthesize pure Mg, Mg–10Al, Mg–15Al, Mg–20Al, and Mg–10Al–1.5Al_2O_3 formulations.
2. Addition of Al particulates lead to the formation of $Mg_{17}Al_{12}$ secondary phase in matrix. Reasonably uniform distribution of secondary phases in the matrix is obtained in the case of Mg–10Al and Mg–10Al–1.5Al_2O_3 samples. In the case of Mg–15Al and Mg–20Al, clusters of secondary phase were additionally observed.
3. The presence of increasing amount of Al leads to an increase in hardness and strengths of pure Mg while failure strain was compromised. However, composite Mg–10Al–1.5Al_2O_3 sample shows an overall improvement in hardness, 0.2%YS, UTS, and failure strain.
4. Fracture behavior of Mg, Mg–10Al, and Mg–10Al–1.5Al_2O_3 samples shows evidence of mixed-mode fracture with the presence of microcracks and limited evidence of plastic deformation. Mg–15Al samples exhibited significant presence of microcracks, and Mg–20Al samples showed flat fracture surface indicative of dominant brittle fracture mode.

Acknowledgements The authors would like to thank Agency for Science, Technology and Research (ASTAR) Grant 0921370015 (WBS R-265-000-321-305) for supporting this research work.

References

1. Shackelford JF (2009) Introduction to materials science for engineers. Pearson Prentice Hall, Upper Saddle River
2. Srivatsan TS, Vasudevan S, Petrorali M (2008) J Alloy Compds 460:386
3. Umeda J, Kawakami M, Kondoh K, Ayman ELS, Imai H (2010) Mater Chem Phys 123:649
4. Dahle AK, Lee YC, Nave MD, Schaer PL, StJohn DH (2001) J Light Metals 1:61
5. Nguyen QB, Gupta M (2008) J Alloy Compds 459:244
6. Wang J, Ding Z, Qi F, Zhu H, Fan Y (2010) J Alloy Compds 507:322
7. Hirai K, Somekawa H, Takigawa Y, Higashi K (2005) Mater Sci Eng A 403:276
8. Yang M, Zhua Y, Lianga X, Pan F (2011) Mater Sci Eng A 528:1721
9. ASM Metals Handbook (1990) Properties and selection nonferrous alloys and special purpose materials, vol 2, 10th edn. ASM Metals Handbook, Metals Park, p 481
10. El-Amoush AS (2008) J Alloy Compds 463:475
11. Trojanová Z, Gärtnerová V, Jäger A, Námešny A, Chalupová M, Palček P, Lukác P (2009) Comp Sci Technol 69:2256
12. Suna M, Wua G, Wang W, Ding W (2009) Mater Sci Eng A 523:145
13. Candan S, Unal M, Koc E, Turen Y, Candan E (2011) J Alloy Compds 509:1958
14. Xie H, Jia L, Zhang J, Wang Z, Lu Z (2009) Mater Sci Eng A 519:204
15. Nguyen QB, Gupta M (2010) Mater Sci Eng A 527:1411
16. Deng KK, Wu K, Wang XJ, Wu YW, Hu XS, Zheng MY, Gan WM, Brokmeier HG (2010) Mater Sci Eng A 527:1630
17. Tun KS, Gupta M (2007) J Comp Sci Technol 67:2657
18. Nguyen QB, Gupta M (2009) J Comp Mater 43:5
19. Hassan SF, Gupta M (2006) J Alloy Compd 419:84
20. Hassan SF, Ho KF, Gupta M (2004) Mater Lett 58:2143
21. Ashby MF (1981) Prog Mater Sci, Bruce Chalmers Anniversary Volume, p 1.
22. Dodd B, Bai Y (1987) Ductile fracture and ductility. Academic Press Inc, Ltd, London